The Mechanism of High Ductility for Novel High-Carbon Quenching–Partitioning–Tempering Martensitic Steel

SHENGWEI QIN, YU LIU, QINGGUO HAO, YING WANG, NAILU CHEN, XUNWEI ZUO, and YONGHUA RONG

In this article, a novel quenching–partitioning–tempering (Q–P–T) process was applied to treat Fe-0.6C-1.5Mn-1.5Si-0.6Cr-0.05Nb hot-rolled high-carbon steel and the microstructures including retained austenite fraction and the average dislocation densities in both martensite and retained austenite were characterized by X-ray diffraction, scanning electron microscopy, and transmission electron microscopy, respectively. The Q–P–T steel exhibits high strength (1950 MPa) and elongation (12.4 pct). Comparing with the steel treated by traditional quenching and tempering (Q&T) process, the mechanism of high ductility for high-carbon Q–P–T steel is revealed as follows. Much more retained austenite existing in Q–P–T steel than in Q&T one remarkably enhances the ductility by the following two effects: the dislocation absorption by retained austenite effect and the transformation-induced plasticity effect. Besides, lower dislocation density in martensite matrix produced by Q–P–T process plays an important role in the improvement of ductility. However, some thin plates of twin-type martensite embedded in dislocation-type martensite matrix in high-carbon Q–P–T steel affect the further improvement of ductility.

I. INTRODUCTION

OVER the past decades, advanced high-strength steels (AHSS) have been developed to reduce the weight of steel parts so that not only save energy and raw materials but also protect the environment. Several kinds of low alloying Fe-Mn-Si-based AHSS, for instance, dual-phase (DP) steels consisting of ferrite and martensite[1,2] and transformation-induced plasticity (TRIP) steels consisting of ferrite, bainite, and retained austenite,[3–6] have been studied intensively. Because of good combination of strength (500 to 1000 MPa) and elongation (15 to 40 pct) as well as relatively high product of strength and elongation (PSE),[7–10] they are more and more applied to automotive industry. For the purpose of achieving higher combination of strength and ductility, a novel heat treatment for producing martensitic steels, named quenching–partitioning (Q&P) process, was proposed by Speer et al.[11–13] The Q&P process involves quenching from austenitizing temperature to a temperature (T_q) between the martensite-start (M_s) and martensite-finish (M_f), followed by a 'partitioning' treatment either at (1-step Q&P) or above (2-step Q&P) T_q temperature, and in the duration of 'partitioning' carbon diffuses from the supersaturated martensite phase to the untransformed austenite phase; therefore, carbon-enriched retained austenite can be stabilized in subsequent cooling to room temperature. For low- or medium-carbon Q&P steels, the T_q is usually much higher than room temperature,[14] and thus considerable retained austenite can be obtained. The low- and medium-carbon steels subjected to Q&P process show excellent strength together with good ductility.

Based on the CCE theory for Q&P process,[11] the precipitation of carbides is not permitted during Q&P process, and therefore it excluded precipitation strengthening. For this reason, Hsu[15] proposed the quenching–partitioning–tempering (Q–P–T) process. Additional carbide-forming elements like Nb and Mo are added in Q–P–T steels, which can lead to carbide formation and grain refinement for precipitation strengthening and refined grain strengthening.[16] Since Q–P–T process absorbs the core idea of Q&P process: quenching temperature (T_q) determined by the combination of CCE theory and K–M equation,[11] the Q–P–T process, from this sense, is also called a modified Q&P one. Obviously, the Q–P–T martensitic steels also have considerable retained austenite comparing with tradition quenching and tempering (Q&T) process (its T_q is room temperature). Our previous researches[17–20] indicate that low-carbon (Fe-0.256C-1.2Si-1.48Mn-1.51Ni-0.053Nb) or medium-carbon (Fe-0.42C-1.46Mn-1.5Si-0.028Nb) Q–P–T steel exhibits much better PSE than low-carbon or medium-carbon Q&T steels due to more retained austenite. The ductility enhanced by retained austenite stems from not only well-known transformation-induced plasticity (TRIP)

SHENGWEI QIN, YU LIU, and QINGGUO HAO, Ph.D. Students, NAILU CHEN and YONGHUA RONG, Professors, and XUNWEI ZUO, Lecturer, are with the School of Materials Science and Engineering, Shanghai Jiao Tong University, Shanghai 200240, P.R. China. Contact e-mail: nlchen@sjtu.edu.cn YING WANG, Lecturer, is with School of Mechanical Engineering, Shanghai Dianji University, Shanghai 200245, P.R. China.
Manuscript submitted January 27, 2015.
Article published online June 26, 2015.

effect[21] and blocking crack propagation (BCP) effect[22] proposed nearly 50 years ago but also a new effect: dislocation absorption by retained austenite (DARA) effect.[20] TRIP effect enhances the ductility by strain-induced martensitic transformation, which relieves the stress within untransformed retained austenite and its adjacent martensite during deformation,[23] and thus TRIP effect delays the necking. The retained austenite blocks crack propagation after necking of tensile sample, *i.e.*, the cracks either grow continuously in the austenite or trace a zig-zag path through interlocking martensite laths, which will require an increased energy for fracture.[22] We proposed DARA effect in medium-carbon Q–P–T steel based on the measurement of average dislocation densities in both martensite and retained austenite during deformation by X-ray diffraction line profile analysis (XLPA), namely, during initial deformation the average dislocation density in martensite decreases with increasing strain and then gradually increases. Such a phenomenon cannot be explained by TRIP and BCP effects; as a result, we proposed DARA effect, that is, dislocations in martensite move into nearby retained austenite through martensite–retained austenite interfaces, and these dislocations are absorbed by retained austenite. The possibility of dislocations transmitted from bcc phase into the fcc phase has been verified by molecular dynamic simulations[24–26] in Cu-Nb bi-layer film.[27] DARA effect makes hard phase martensite to be a "softening" state during deformation and effectively enhances the deformation ability of martensite matrix. The more the retained austenite is, the more obvious the DARA, TRIP, and BCP effects are, and thus the higher the ductility is. Two empirical conditions of remarkable DARA effect were further proposed: (1) the enough amount of retained austenite, being larger than 10 pct volume fraction; and (2) the interface between two phases should be coherent or semi-coherent. These two conditions were confirmed by low-carbon Q–P–T steel[19] and bainitic steel,[18] respectively, in which the interface between martensite (or bainite) and retained austenite was coherent or semi-coherent at K–S or N–W orientation relationship.

In low- or medium-carbon Q–P–T steels, martensite is dislocation-type one, if in a high-carbon Q–P–T steel twin-type martensite will partially replace dislocation-type martensite; how about DARA effect and TRIP effect in such a condition is an issue we concern on. Another issue is whether Q–P–T process can markedly improve the ductility of high-carbon steel or not by comparing with traditional high-carbon Q&T martensitic steels, whose elongation is usually less than 10 pct. In this work, a high-carbon steel was treated by a novel Q–P–T process and traditional Q&T process, and the above two issues will be focused in this study by comparing the mechanical properties and microstructures of Q–P–T steel with those of Q&T steel.

II. EXPERIMENTAL PROCEDURES

The composition of the steel studied was chemically analyzed as Fe-0.63C-1.52Mn-1.49Si-0.62Cr-0.036Nb. The principles of compositional design for this high-strength steel are described as follows. Carbon and manganese in the steel are added to increase the stability of austenite due to lowering the M_s.[28] Silicon can suppress the precipitation of brittle cementite (Fe_3C) in the course of tempering.[29] Alloying elements Nb and Cr can lead to stable carbide formation, in which Nb also can effectively refine grains.[15,30] The A_{c3} and M_s temperatures were, respectively, determined to be 1053 K and 498 K (780 °C and 225 °C) by a Gleeble-3500 thermal simulator.

The designed steel was melted in a medium frequency furnace, and a hot-rolled plate with 20 mm thickness was prepared by the Central Iron and Steel Research Institute, Beijing, China. Specimens with 2 mm thickness were cut from the hot-rolled plate. After cutting, some of the specimens were subjected to the Q–P–T process, which involves austenitizing at 1103 K (830 °C) for 300 seconds, followed by quenching in a salt bath at 433 K (160 °C) (T_q) for 10 seconds, then partitioning and tempering at 673 K (400 °C) for 60 seconds in molten salt, and finally quenching to room temperature in water. Other specimens were subjected to the Q&T process: directly quenched to room temperature in water from 1103 K (830 °C) and then tempering at 673 K (400 °C) for 60 seconds in molten salt. The difference between Q–P–T process and Q&T process is only quenching temperature (T_q), and the former is higher than the latter (room temperature).

Rectangular tensile specimens were cut to the gage length of 15 mm, thickness of 1.5 mm, and width of 5 mm. Tensile tests were executed on Zwick/Roell Z100 universal testing machine at a strain rate of 2×10^{-3} s^{-1} at room temperature. Specimens for transmission electron microscopy (TEM) were prepared by mechanically polishing and then electropolishing in a twin-jet polisher using 4 pct perchloric acid and 96 pct ethanol from 253 K to 243 K (−20 °C to −30 °C). TEM was performed in a JEOL-2100F microscope operated at 200 kV. The volume fractions of retained austenite (V_{RA}) in the Q–P–T samples at different strain stages were measured by X-ray diffraction (XRD) with CuKα radiation using a D/max-2550 X-ray diffractometer based on a direct comparison method of the integrated intensity of the austenite $(200)_\gamma$, $(220)_\gamma$, and $(311)_\gamma$ peaks and the martensite $(200)_\alpha$ and $(211)_\alpha$ peaks.[31] The average dislocation densities in both martensite and retained austenite were measured by XLPA, rather than TEM because the TEM method produces a localized value without statistical information. Both the average dislocation density ($\bar{\rho}_M$ for martensite, $\bar{\rho}_A$ for austenite) and microstrain ($(\varepsilon_M^2)^{1/2}$ for martensite, $(\varepsilon_A^2)^{1/2}$ for austenite) were determined by XLPA, which is in detail described in References 32,33. The selected reflections of $(200)_\gamma$ and $(211)_\alpha$ were slowly scanned with a velocity of 0.2 deg/min to make sure to acquire sufficient diffraction intensity and a good profile for XLPA. Instrumental correction was carried out using the powder patterns of an Fe standard and a sol–gel Fe-32Ni (wt pct) austenite standard and the Ni and Stokes correction procedure.[34] The main error sources of the dislocation density measurement are the magnitude of the diffraction intensity and the diffraction peak profile. Compared

with the $(200)_\gamma$ peak of retained austenite, the $(211)_\alpha$ peak of martensite exhibits much higher intensity and a better profile, and hence the measurement error for the average dislocation density in martensite is much less than that in retained austenite.

III. RESULTS

A. Measurement of Mechanical Properties

The tensile tests of Q–P–T and Q&T samples were performed, respectively, and their engineering stress–strain curves in Figure 1 indicate that the Q–P–T steel exhibits high tensile strength of 1950 MPa and a total elongation of 12.4 pct accompanying high PSE of 24180 MPa pct. The tensile result of Q&T steel samples shows a tensile strength of 2360 MPa and a total elongation of 6.1 pct accompanying low PSE of 14396 MPa pct. It can be seen that novel Q–P–T process prominently improves the PSE of high-carbon steel when comparing with traditional Q&T process, while PSE (energy unit), as a comprehensive property, is traditionally considered to represent the properties of toughness.[35] Comparing the tensile curve of Q–P–T steel with that of Q&T one, it can be found that the elongation (uniform deformation) corresponding to the tensile strength is 11.6 pct for
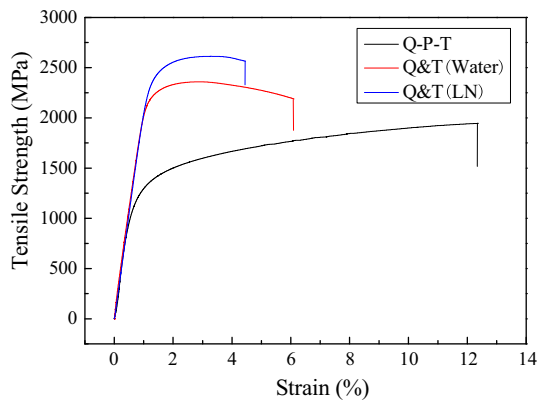

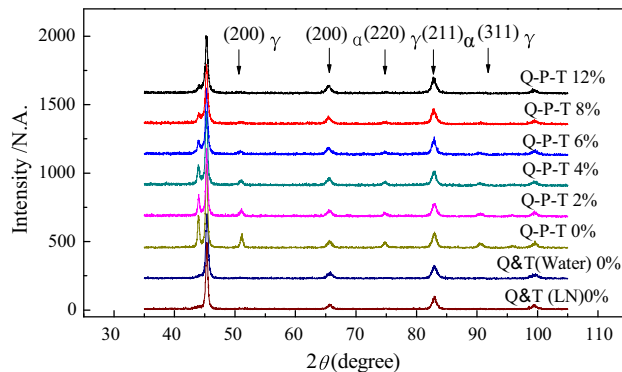Fig. 1—Engineering stress–strain curves of Q–P–T and Q&T samples.

Fig. 2—XRD spectra of the Q–P–T and Q&T tensile samples at different strain stages (from 0 to 12.4 pct strains).

Q–P–T steel and 1.9 pct for Q&T steel, and the elongation after necking is 0.8 pct for Q–P–T steel and 4.2 pct for Q&P, which implies different necking behaviors.

B. Characterization of Microstructures

Based on the XRD spectra of Q–P–T and Q&T samples before tensile test (0 pct) in Figure 2, their microstructures are determined as bcc phase and fcc phase. The volume fraction of fcc phase is determined to be 29.1 pct in Q–P–T sample and 7.1 pct in Q&T sample. TEM characterization further indicates that the bcc phase consists of dislocation-type martensite plates and some thin plates of twin-type martensite embedded in them, as shown by the bright-field (BF) image in Figure 3(a), in which twin-type martensite is identified by the combination of dark-field (DF) images in Figures 3(b) and 4(b) and selected area electron diffraction (SAED) patterns inserted in them. While, the fcc phase is flake-like retained austenite, as shown in Figures 3(c) and (d) for Q–P–T specimen and in Figures 4(c) and (d) for Q&T specimen. Moreover, the SAED patterns in Figures 3(d) and 4(d) both show the $(1\bar{1}0)_\alpha//(\bar{1}\bar{1}1)_\gamma$, $[\bar{1}11]_\alpha//[011]_\gamma$ (K–S) and $(\bar{1}\bar{1}0)_\alpha//(\bar{1}\bar{1}1)_\gamma$, $[00\bar{1}]_\alpha//[011]_\gamma$ (N–W) orientation relationship between martensite and retained austenite. The carbides distributed in martensite matrix were identified as NbC, and the orientation relationship between NbC and martensite was determined, respectively, as $(100)_\alpha//(110)_{MC}$, $[01\bar{1}]_\alpha//[\bar{1}10]_{MC}$ (B-N) and $(01\bar{1})_\alpha//(\bar{4}20)_{MC}$, $[\bar{1}11]_\alpha//[\bar{1}22]_{MC}$, as shown in Figures 3(f) and 4(f).

IV. DISCUSSION

A. DARA Effect

Our previous studies indicate that low- or medium-carbon Q–P–T martensitic steels consist of dislocation-type martensite matrix and considerable retained austenite; moreover, there are K–S or/and N–W orientation relationships between martensite and retained austenite, and thus there is DARA effect during deformation,[18–20] while in low- or medium-carbon Q&T martensitic steels there is no DARA effect during deformation due to the few amount of retained austenite (less than 3 pct volume fraction).[20] For high-carbon martensitic steels studied in this work, there are some thin plates of twin-type martensite, and they are embedded in dislocation-type martensite matrix. Since twin boundaries can block the movement of dislocations, can they suppress DARA effect during deformation? In order to answer this question, the microstrains and the average dislocation densities in both martensite and retained austenite in Q–P–T samples at different strain stages were measured by XLPA (Table I), in which two samples were measured at each strain and the average dislocation density($\bar{\rho}_M$ or $\bar{\rho}_A$) was obtained. During deformation, both $\bar{\rho}_M$ and $\bar{\rho}_A$ are expected to increase with increasing strain owing to dislocation multiplication, but the XLPA results were out of our expectation. The $(\varepsilon_A^2)^{1/2}$ and $\bar{\rho}_A$ in the retained austenite
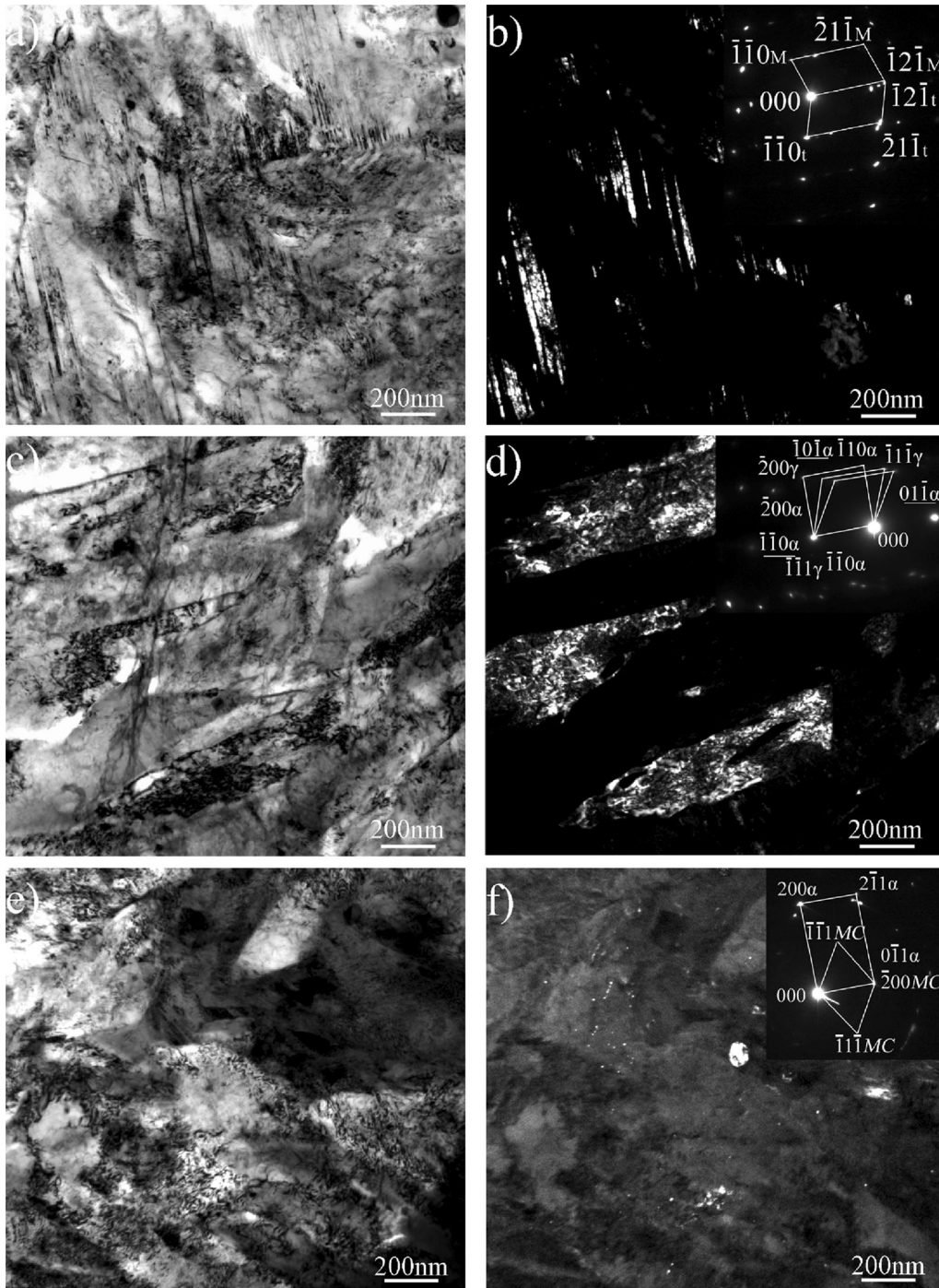
Fig. 3—TEM micrographs of undeformed Q–P–T sample: (*a*) twinning martensite, BF image, (*b*) twinning martensite, DF image and inserted SAED pattern (incident beam direction $z \approx [113]_M$ or $[1\bar{1}3]_t$), (*c*) BF image of Q–P–T sample, (*d*) DF image of retained austenite and inserted SAED pattern of the retained austenite and martensite (incident beam direction $z \approx [011]_\gamma$ or $[\bar{1}11]_\alpha$), (*e*) BF images, and (*f*) DF images and inserted SAED pattern of niobium carbides (incident beam direction $z \approx [01\bar{1}]_\alpha$ or $[\bar{1}10]_{MC}$).

rapidly increase with raising the strain; however, $\left(\varepsilon_M^2\right)^{1/2}$ and $\bar{\rho}_M$ in martensite did not change in the same way. For instance, before tensile test, $\left(\varepsilon_M^2\right)^{1/2}$ and $\bar{\rho}_M$ were 3.05×10^{-3} and 11.44×10^{14} m^{-2}, while $\left(\varepsilon_M^2\right)^{1/2}$ and $\bar{\rho}_M$ were 2.92×10^{-3} and 10.80×10^{14} m^{-2} at 4 pct strain, respectively, which were less than those before tensile test. Obviously, such a phenomenon cannot be explained by TRIP or BCP effects. During initial deformation, the $\bar{\rho}_M$ in martensite reduces with increasing strain, indicating that the amount of dislocation transported to retained austenite is larger than that of the dislocation multiplication in martensite, and then after 6 pct strain the $\bar{\rho}_M$ in martensite gradually rises with increasing strain, indicating that the amount of dislocation transported to retained austenite is less than
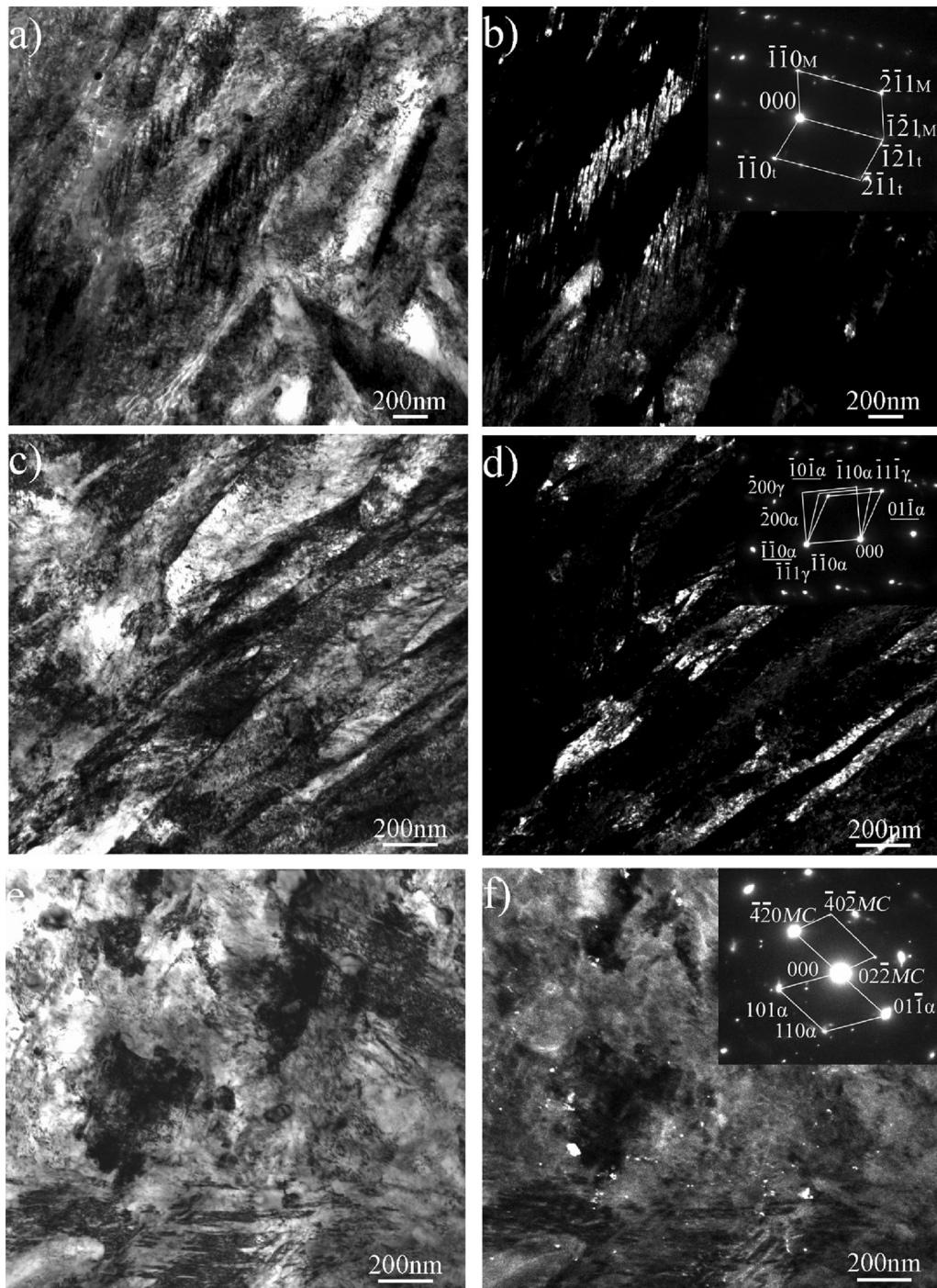
Fig. 4—TEM micrographs of undeformed Q&T sample: (*a*) twinning martensite, BF image, (*b*) twinning martensite, DF image and inserted SAED pattern (incident beam direction $z \approx [113]_M$ or $[\bar{1}\bar{1}3]_t$), (*c*) BF image of Q&T sample, (*d*) DF image of retained austenite and inserted SAED pattern of the retained austenite and martensite (incident beam direction $z \approx [011]_\gamma$ or $[\bar{1}11]_\alpha$), (*e*) BF images, and (*f*) DF images and inserted SAED pattern of niobium carbides (incident beam direction $z \approx [\bar{1}11]_\alpha$ or $[\bar{1}22]_{MC}$).

that of the dislocation multiplication in martensite. The variation of the average dislocation density in martensite with strain is plotted in Figure 5(a), while that in retained austenite is plotted in Figure 5(b). For high-carbon Q&T sample, the variation of dislocation density in martensite with strain was observed in the similar tendency, also shown in Figure 5(a). However, the drop maximum (0.80×10^{14} m^{-2}) of the average dislocation

density in Q&T sample is much less 1.98×10^{14} m^{-2} in Q–P–T sample when comparing with the average dislocation density before tensile test, which indicates a weak DARA effect in Q&T steel due to less retained austenite fraction compared with Q–P–T steel. Moreover, the average dislocation densities (11.44×10^{14} m^{-2}) in martensite for Q–P–T samples are much less than 16.40×10^{14} m^{-2} for Q&T sample before

Table I. Microstructural Parameters of Martensite and Retained Austenite in Q–P–T Tensile Samples at Different Strain Stages

| Process	Strain (pct)	$(\varepsilon_M^2)^{1/2}\ (\times 10^{-3})$	ρ_{M1}	ρ_{M2}	$\bar{\rho}_M\ (\times 10^{14}\,\mathrm{m}^{-2})$	$(\varepsilon_A^2)^{1/2}\ (\times 10^{-3})$	ρ_{A1}	ρ_{A1}	$\bar{\rho}_A\ (\times 10^{14}\,\mathrm{m}^{-2})$	V_{RA} (pct)
Q–P–T	0	3.05 ± 0.03	12.48 ± 0.15	10.40 ± 0.13	11.44 ± 0.13	1.93 ± 0.16	16.67 ± 1.05	9.99 ± 0.63	13.33 ± 0.84	29.1
	2	2.94 ± 0.06	12.00 ± 0.26	10.00 ± 0.22	11.00 ± 0.24	2.39 ± 0.15	22.03 ± 1.30	13.23 ± 0.78	17.63 ± 1.04	25.9
	4	2.92 ± 0.06	11.78 ± 0.32	9.82 ± 0.26	10.80 ± 0.29	2.68 ± 0.21	26.01 ± 2.54	15.61 ± 1.52	20.81 ± 2.03	20.4
	6	2.65 ± 0.10	10.32 ± 0.40	8.60 ± 0.34	9.46 ± 0.37	3.28 ± 0.20	43.80 ± 2.59	26.28 ± 1.55	35.04 ± 2.07	17.9
	8	2.91 ± 0.05	11.03 ± 0.24	9.19 ± 0.20	10.11 ± 0.22	3.88 ± 0.59	55.78 ± 10.15	33.46 ± 6.09	44.62 ± 8.12	15.1
	12.40	2.93 ± 0.06	11.81 ± 0.32	9.85 ± 0.26	10.83 ± 0.29					10.4
Q&T (water)	0	3.59 ± 0.06	17.89 ± 0.34	14.91 ± 0.28	16.40 ± 0.31					
	3	3.52 ± 0.05	17.02 ± 0.34	14.18 ± 0.28	15.60 ± 0.31					
	6.10	3.57 ± 0.54	17.46 ± 0.24	14.54 ± 0.20	16.00 ± 0.22					
Q&T (LN)	0	3.38 ± 0.06	16.08 ± 0.30	13.40 ± 0.36	14.74 ± 0.33					
	2	3.54 ± 0.07	17.30 ± 0.35	14.42 ± 0.41	15.86 ± 0.38					
	4	3.91 ± 0.06	19.88 ± 0.37	16.56 ± 0.45	18.22 ± 0.41					
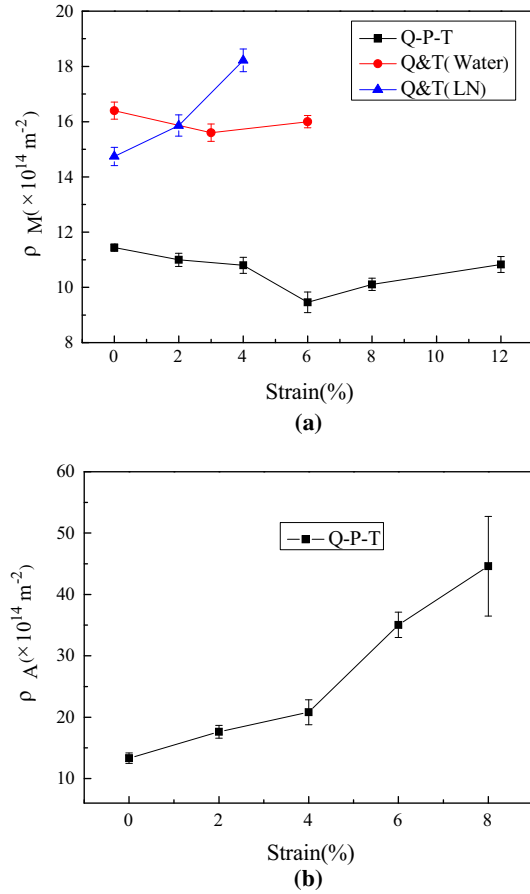
Fig. 5—The variation of average dislocation density with strain in martensite or retained austenite in Q–P–T sample or Q&T one.

tensile test. Therefore, Q–P–T sample keeps low dislocation density at whole deformation comparing with Q&T sample. In order to further clarify the DARA effect of the Q–P–T steels in this research, we at first replenished an investigation on two Q&T samples after deep cooling by liquid nitrogen, but there is still about 5 pct volume fraction of retained austenite and weak DARA effect, so we took the following process: two high-carbon samples were direct quenched in liquid nitrogen (LN) to get rid of the effect of retained austenite as possible. The diffraction peaks of retained austenite cannot be found in XRD spectrum for LN sample, as shown in Figure 2. The microstrains and the average dislocation densities in martensite for LN samples at different strain stages were also measured by XLPA (Table I), and the variation of average dislocation densities in martensite with strain is plotted in Figure 5(a). Figure 5(a) shows that the average dislocation densities in martensite monotonously increase with increasing strain, indicating that there is no DARA effect in LN sample due to no retained austenite. It could be a direct evidence for the DARA effect in the retained austenite-contained Q–P–T steels. The total elongation of LN sample is only about 5 pct although the tensile strength is high up to 2500 MPa (Figure 1). In order to estimate the amount of dislocation in martensite transported to retained austenite, the following
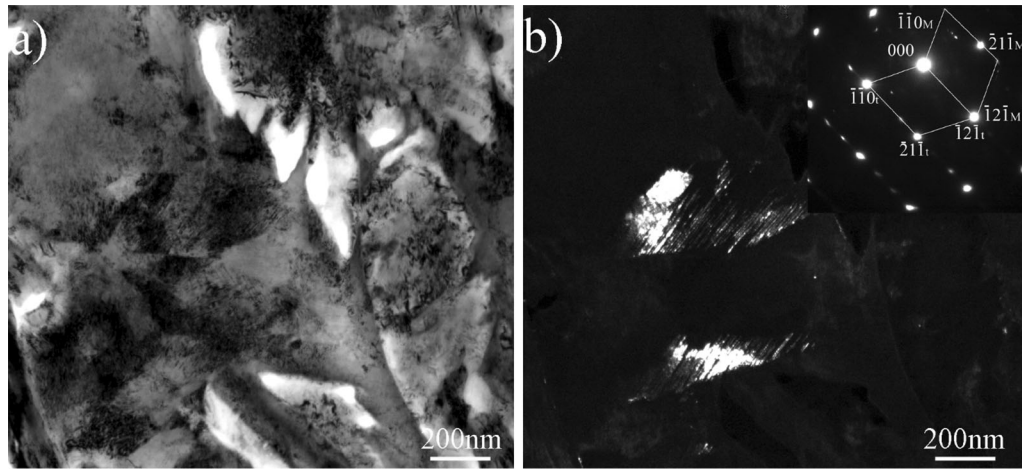
Fig. 6—TEM micrographs of strain-induced twinning martensite in deformed Q–P–T specimen: (*a*) bright-field image and (*b*) dark-field image and inserted SAED pattern (incident beam direction $z \approx [113]_M$ or $[\bar{1}1\bar{3}]_t$).

calculation is simply done. During 4 pct deformation, the increase of the average dislocation density in martensite for LN sample is about 3.48×10^{14} m^{-2} (see Table I) owing to dislocation multiplication when comparing with that in the sample before deformation. The drop amount of dislocation in martensite is about 0.58×10^{14} m^{-2} at 4 pct strain (see Table I) for Q–P–T sample, and thus the total amount of dislocation in martensite transported to retained austenite is about 4.06×10^{14} m^{-2} due to DARA effect if the increase of the average dislocation density in martensite is assumed to be 3.48×10^{14} m^{-2} in Q–P–T sample due to dislocation multiplication as the same as LN sample. Such a value (4.06×10^{14} m^{-2}) is rather large, which occupies about 30 pct of the value (11.44×10^{14} m^{-2}) of the initial dislocation density before tensile testing (0 pct strain), and is over two times of the increase (1.90×10^{14} m^{-2}) of the average dislocation density in the pure aluminum at 8 pct true strain.[36]

Since the variation tendency of dislocation density with strain in martensite for this high-carbon Q–P–T steel is similar to low- or medium-carbon Q–P–T steels, it is reasonably believed that the thin plates of twin-type martensite embedded in dislocation-type martensite matrix does not suppress the DARA effect, which probably results from too small amount of twin-type martensite. While, in high-carbon Q&T martensitic steels there is still weak DARA effect during deformation, which is different from low- or medium-carbon Q&T steels. The difference is attributed to relative more retained austenite fraction (7.1 pct) in high-carbon Q&T steel than in low- or medium-carbon Q&T steels (less than 3 pct). When the high-carbon steel is quenched in liquid nitrogen, DARA effect disappears in the LN sample due to no retained austenite, and this experiment on the other side supports the presence of DARA effect in Q–P–T steels.

B. TRIP Effect

In our previous study, the variation of the V_{RA} with strain in medium-carbon Q–P–T steel exhibits remarkable TRIP effect, namely, the V_{RA} gradually decreases from 16, 13, 10, and 5 to 3 pct with the increase of strain from 0 (before deformation), 3, 7, and 11 to 15 pct, respectively.[20] The V_{RA} (29.1 pct) in this high-carbon Q–P–T steel is much more than 16 pct in the medium-carbon Q–P–T steel before tensile test, and the issue we face is: whether more retained austenite can produce more remarkable TRIP effect in high-carbon Q–P–T steel than in medium-carbon Q–P–T steel or not? For the reason, the V_{RA} in tensile samples with different strains from 0 to 12 pct was measured by XRD (Figure 2), and the results are listed in Table I. It is quite clear from Table I that the V_{RA} gradually decreases from 29.1, 25.9, 20.4, 17.9, and 15.1 to 10.4 pct with increasing stain from 0, 2, 4, 6, and 8 to 12.4 pct, respectively, which exhibits TRIP effect. TRIP effect gradually occurs during deformation accompanying with the decrease of the V_{RA}. The TRIP effect was confirmed by TEM observation. Since retained austenite in Q–P–T steel has more than 0.8 wt pct carbon content, the strain-induced martensite is twin-type martensite.[37] Figure 6 shows TEM micrographs of strain-induced twinning martensite in deformed Q–P–T specimen after fracture. Comparing Figure 6 with Figure 3, it is found that the strain-induced twinning martensite during deformation is different from thermal-induced twinning martensite during quenching (comparing Figure 6(b) with Figure 3(b)), and the former is shorter than the latter in length since the strain-induced twinning martensite is limited in retained austenite. It is worthy to point out that 10.4 pct retained austenite in high-carbon Q–P–T sample has not transformed to martensite at the fracture of tensile sample, being much more than 3 pct retained austenite in medium-carbon Q–P–T steel, which implies that TRIP effect has not fully contributed to the ductility of high-carbon Q–P–T steel. It is concluded that more retained austenite in high-carbon Q–P–T steel than medium-carbon Q–P–T steel cannot produce stronger TRIP effect.

C. Mechanism of High Ductility

Comparing the mechanical properties of high-carbon Q–P–T steel with those of Q&T steel, we can find that
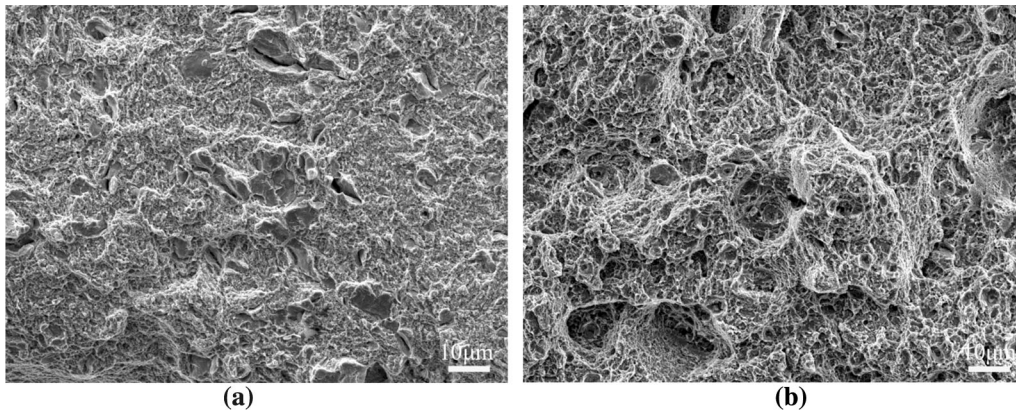
Fig. 7—SEM fracture photographs of the samples after different heat treatment processes: (*a*) Q&T sample and (*b*) Q–P–T sample.

the uniform elongation (11. 6 pct) of Q–P–T steel is much higher than 1.9 pct of Q&T. Obviously, the high ductility stems from much more V_{RA} in Q–P–T steel than in Q&T steel. The above results indicate that the ductility is enhanced by retained austenite through two approaches: DARA effect and TRIP effect. The DARA effect makes the hard phase martensite in a "softening" state during whole deformation, availably intensifies the deformation ability of the hard phase martensite at uniform deformation stage, and in turn evidently improves the ductility. Since not every martensite grain (lath) would have an adjacent retained austenite, the dislocations only in martensite lath neighboring retained austenite can move into the retained austenite. As a result, the more the V_{RA} is, the stronger the DARA effect is. With further increase of strain, the strain-induced martensitic transformation from retained austenite will occur when the stress caused by high density of dislocation in local area reaches certain critical value, and this leads to TRIP effect because strain-induced martensitic transformation relaxes the stress concentration in this area and avoids the formation of cracks effectively, and thus delays the necking of the Q–P–T steel. Obviously, the more the retained austenite is, the stronger the TRIP effect is. It is worthy to point out that BCP effect hardly contributes the ductility of Q–P–T steel because the elongation after necking is only 0.8 pct, but BCP effect contributes to the ductility of Q&T steel because the elongation after necking is high up to 4.2 pct, occupying about 70 pct of total elongation. The high ductility of high-carbon Q–P–T steel is not only attributed to more retained austenite but also attributed to lower dislocation density in martensite than high-carbon Q&T steel (see Table I). By comparison of the fracture morphologies of high-carbon Q–P–T sample with those of high-carbon Q&T steel (see Figure 7), the tearing ridges in Q–P–T sample are more than those in Q&T sample, which probably results from more soft phase retained austenite, and the dimples in Q–P–T sample are deeper than those in Q&T sample, which probably results from lower dislocation density in martensite matrix.

Although high-carbon Q–P–T martensitic steel exhibits higher ductility than high-carbon Q&T marten-

sitic steel, its total elongation is much less than that of medium-carbon Q–P–T steel in our previous study.[20] Medium-carbon Q–P–T steel has only 16 pct V_{RA}, much less than 29.1 pct in high-carbon Q&T steel, but the total elongation of medium-carbon Q–P–T steel is high up to 20 pct, being much higher than 12.4 pct of high-carbon Q–P–T steel. Therefore, it is reasonably believed that the ductility of a martensitic steel is mainly not dependent on the amount of soft phase retained austenite, but is dependent on the abilities of the deformation and hindering crack formation of hard phase martensite matrix. Detailed analysis will be described as follows. The average dislocation density in martensite matrix for high-carbon Q–P–T steel is much less than that for high-carbon Q&T steel, and this is attributed to the decrease of carbon content during partitioning of carbon from martensite to retained austenite accompanying the reduction of dislocation density. Martensite matrix with lower dislocation density has stronger deformation ability. However, there are thin plates of twin-type martensite in high-carbon Q–P–T steel, and these thin plates are embedded in dislocation-type martensite matrix. Since twin boundaries can effectively block the movement of dislocations during deformation, dislocations piling-up at twin boundaries will cause the concentration of stress, which leads to the preferential formation of cracks at twin boundaries. Accordingly, it is reasonably believed that secondary microcracks in high-carbon Q–P–T and Q&T steels, as shown in Figure 7, are mainly caused by thin plates of twin-type martensite, and thin plates of twin-type martensite promote the crack formation in dislocation-type martensite matrix and weaken the resistance of crack formation. This is why TRIP effect has not fully contributed to the ductility of high-carbon Q–P–T steel.

In general, a novel Q–P–T process makes high-carbon steel obtain more retained austenite than traditional Q&T process, and retained austenite remarkably enhances the ductility of high-carbon Q–P–T steel by DARA effect and TRIP effect. Besides, carbon diffuses from the supersaturated martensite phase to the untransformed austenite phase during Q–P–T process, which leads to lower dislocation density in martensite matrix and effectively intensifies the deformation ability

of hard phase martensite matrix. However, there are thin plates of twin-type martensite in high-carbon Q–P–T steel, and they will cause the preferential formation of cracks at twin boundaries and affect the further improvement of ductility.

V. CONCLUSIONS

Fe-0.6C-1.5Mn-1.5Si-0.6Cr-0.05Nb high-carbon steel designed was treated by novel Q–P–T (also called modified Q&P) process and traditional Q&T process. Their mechanical properties were measured and microstructures were characterized by XRD, SEM, and TEM. The mechanism of high ductility of high-carbon Q–P–T steel was revealed by comparison of high-carbon Q&T steel. Main conclusion will be described as follows:

1. High-carbon steel treated by novel Q–P–T process obtains 29.1 pct volume fraction of retained austenite, while the steel by traditional Q&T process obtains only 7.1 pct volume fraction of retained austenite.
2. The XLPA measurement of the average dislocation densities in both martensite and retained austenite for high-carbon Q–P–T sample reveals that there is a strong DARA effect during deformation, while in high-carbon Q&T sample there is weak DARA effect and in the high-carbon LN sample there is no DARA effect; DARA effect effectively intensifies the deformation ability of martensite matrix accompanying with the improvement of ductility.
3. TRIP effect in high-carbon Q–P–T steel was revealed by the measurement of retained austenite fraction at different strains and confirmed by strain-induced twin martensite during deformation; TRIP effect relaxes the stress concentration in local area and avoids the formation of cracks and thus enhances ductility.
4. By comparing with Q&T steel, the high ductility of high-carbon Q–P–T steel is attributed to (a) more retained austenite accompanying stronger DARA effect and TRIP effect and (b) lower dislocation density in martensite matrix, which enhances the deformation ability of martensite matrix.
5. Thin plates of twin-type martensite in high-carbon Q–P–T steel cause the preferential formation of cracks at twin boundaries and affect the further improvement of ductility.

REFERENCES

1. A.-P. Pierman, O. Bouaziz, T. Pardoen, P.J. Jacques, and L. Brassart: *Acta Mater.*, 2014, vol. 73, pp. 298–311.
2. M. Sarwar and R. Priestner: *J. Mater. Sci.*, 1996, vol. 31, pp. 2091–95.
3. B.C. De Cooman: *Curr. Opin. Solid State Mater. Sci.*, 2004, vol. 8, pp. 285–303.
4. P.J. Jacques: *Curr. Opin. Solid State Mater. Sci.*, 2004, vol. 8, pp. 259–65.
5. L. Li, P. Wollants, Y.L. He, B.C. De Cooman, X.C. Wei, and Z.Y. Xu: *Acta Metall. Sin.*, 2009, vol. 16, pp. 457–65.
6. C. Ouchi: *ISIJ Int.*, 2001, vol. 41, pp. 542–53.
7. P.J. Jacques, Q. Furnémont, F. Lani, T. Pardoen, and F. Delannay: *Acta Mater.*, 2007, vol. 55, pp. 3681–93.
8. F. Lani, Q. Furnémont, T. Van Rompaey, F. Delannay, P.J. Jacques, and T. Pardoen: *Acta Mater.*, 2007, vol. 55, pp. 3695–705.
9. A.K. Srivastava, G. Jha, N. Gope, and S.B. Singh: *Mater. Charact.*, 2006, vol. 57, pp. 127–35.
10. J. Mahieu, B.C. De Cooman, and J. Maki: *Metall. Mater. Trans. A*, 2002, vol. 33A, pp. 2573–80.
11. J. Speer, D.K. Matlock, B.C. De Cooman, and J.G. Schroth: *Acta Mater.*, 2003, vol. 51, pp. 2611–22.
12. J.G. Speer, D.V. Edmonds, F.C. Rizzo, and D.K. Matlock: *Curr. Opin. Solid State Mater. Sci.*, 2004, vol. 8, pp. 219–37.
13. D.V. Edmonds, K. He, F.C. Rizzo, B.C. De Cooman, D.K. Matlock, and J.G. Speer: *Mater. Sci. Eng., A*, 2006, vol. 438, pp. 25–34.
14. K. Zhang, X. Weizong, Z. Guo, Y. Rong, M. Wang, and H. Dong: *Acta Metall. Sin.*, 2011, vol. 47, pp. 489–96.
15. T.Y. Hsu and Z.Y. Xu: *Mater. Sci. Forum, (Trans Tech Publ: 2007)*, 2007, vols. 561–565, pp. 2283–86.
16. S. Zhou, K. Zhang, Y. Wang, J.F. Gu, and Y.H. Rong: *Mater. Sci. Eng., A*, 2011, vol. 528, pp. 8006–12.
17. S. Zhou, K. Zhang, Y. Wang, J.F. Gu, and Y.H. Rong: *Metall. Mater. Trans. A*, 2012, vol. 43A, pp. 1026–34.
18. Y. Wang, K. Zhang, Z. Guo, N. Chen, and Y. Rong: *Mater. Sci. Eng., A*, 2012, vol. 552, pp. 288–94.
19. Y. Wang, K. Zhang, Z. Guo, N. Chen, and Y. Rong: *Acta Metall. Sin.*, 2012, vol. 48, pp. 641–48.
20. K. Zhang, M. Zhang, Z. Guo, N. Chen, and Y. Rong: *Mater. Sci. Eng., A*, 2011, vol. 528, pp. 8486–91.
21. V.F. Zackay, E.R. Parker, D. Fahr, and R. Busch: *ASM Trans. Q.*, 1967, vol. 60, pp. 252–59.
22. D. Webster: *ASM Trans. Q.*, 1968, vol. 61, pp. 816–28.
23. F. Rui, Z. Meihan, C. Nailu, Z. Xunwei, and R. Yonghua: *Acta Metall. Sin.*, 2014, vol. 50, pp. 498–506.
24. R.F. Zhang, J. Wang, I.J. Beyerlein, and T.C. Germann: *Scripta Mater.*, 2011, vol. 65, pp. 1022–25.
25. J. Wang, A. Misra, R.G. Hoagland, and J.P. Hirth: *Acta Mater.*, 2012, vol. 60, pp. 1503–13.
26. G. Lasko, D. Saraev, S. Schmauder, and P. Kizler: *Comput. Mater. Sci.*, 2005, vol. 32, pp. 418–25.
27. S. Shao and S.N. Medyanik: *Modell. Simul. Mater. Sci. Eng.*, 2010, vol. 18, p. 055010.
28. S.-J. Kim, C.G. Lee, I. Choi, and S. Lee: *Metall. Mater. Trans. A*, 2001, vol. 32A, pp. 505–14.
29. J.H. Jang, I.G. Kim, and H.K.D.H. Bhadeshia: *Comput. Mater. Sci.*, 2009, vol. 44, pp. 1319–26.
30. B.-J. Lee: *CALPHAD*, 1992, vol. 16, pp. 121–49.
31. Mikhail Aleksandrovich Krivoglaz, 1969.
32. W. Woo, L. Balogh, T. Ungár, H. Choo, and Z. Feng: *Mater. Sci. Eng., A*, 2008, vol. 498, pp. 308–13.
33. W. Li, X. Weizong, X. Wang, and Y. Rong: *J. Alloy. Compd.*, 2009, vol. 474, pp. 546–50.
34. A.R. Stokes : *Proc. Phys. Soc.*, 1948, vol. 61, p. 382.
35. R.O. Ritchie: *Nat. Mater.*, 2011, vol. 10, pp. 817–22.
36. J. Gubicza, N. Chinh, Z. Horita, and T. Langdon: *Mater. Sci. Eng., A*, 2011, vol. 387, pp. 55–59.
37. G. Krauss: *Metall. Mater. Trans. A*, 2001, vol. 32A, pp. 861–77.